Title:

Thermo-Hydro-Mechanical Modeling of Geothermal Energy Systems in Deep Mines: Uncertainty Quantification and Design Optimization

Authors:
- [Le Zhang], [Ghent University]
- [Anne-Catherine Dieudonné], [Delft University of Technology]
- [Alexandros Daniilidis], [Delft University of Technology]
- [Longjun Dong], [Central South University]
- [Wenzhou Cao], [Utrecht University]
- [Robin Thibaut], [Lawrence Berkeley National Laboratory]
- [Luka Tas], [Ghent University]
- [Thomas Hermans], [Ghent University]

Statement:
This paper is a non-peer reviewed preprint submitted to EarthArXiv. The preprint has been submitted to the journal "Applied Energy" for peer review.

Thermo-Hydro-Mechanical Modeling of Geothermal Energy Systems in Deep Mines: Uncertainty Quantification and Design Optimization

Le Zhang[1,2], Anne-Catherine Dieudonné[2], Alexandros Daniilidis[2], Longjun Dong[3], Wenzhuo Cao[4], Robin Thibaut[1,5], Luka Tas[1], and Thomas Hermans[1]

[1]Department of Geology, Ghent University, Ghent, Belgium
[2]Faculty of Civil Engineering and Geosciences, Delft University of Technology, Delft, The Netherlands
[3]School of Resources and Safety Engineering, Central South University, Changsha, China
[4]Department of Earth Sciences, Utrecht University, Utrecht, The Netherlands
[5]Lawrence Berkeley National Laboratory, Berkeley, CA, USA

May 6, 2024

Abstract

Exploiting geothermal energy using existing deep mining systems streamlines the development of geothermal systems while addressing the cooling needs of deep mines. However, the combined effects of low-temperature and high-pressure injection during geothermal operations adversely impact the stability of deep mine drifts. This makes it crucial to reliably assess the stability of the drifts and ensure the desired temperature evolution near drifts and the production well. In this paper, we investigate the impact of deep geothermal operations on the stability of mine drifts through thermo-hydro-mechanical (THM) numerical modeling. The results show that impact of cold water injection on the stability of the mine is predominantly influenced by thermal effects, in addition to poro-elastic effects. The reduction in temperature and the increase in pore pressure both contribute to a decrease in effective stress, which is detrimental to the drift stability, though the evolution of the different mechanisms differs. Furthermore, we utilize the distance-based generalized sensitivity analysis (DGSA) method to quantify the sensitivity of the THM model parameters (including design parameters and material properties), thereby optimizing the system design. The results show that the distance between the mine system and the geothermal system is the paramount factor influencing the system's response. Other design parameters (injection rate and temperature, well spacing) and material properties (thermal expansion coefficient, permeability, Young's modulus and heat capacity) also hold substantial significance. Conversely, the system's behaviour is not sensitive to parameters such as porosity and thermal conductivity. By analyzing the range of parameters using DGSA, we provide recommendations for optimizing the system. The verification results show that, given favorable geological settings as suggested, rational selection of system design parameters can facilitate efficient geothermal extraction activities in deep mines. This approach finds optimized development options considering uncertainty of the subsurface, offering valuable advice and guidance for decision-making in geothermal production.

Keywords: Deep Geothermal; Thermo-hydro-mechanical coupling; Sensitivity analysis; Uncertainty quantification.

1 Introduction

With the increasing demand for alternative energy and mineral resources, and the gradual depletion of shallow resources, resource extraction is gradually advancing to deeper geological formations. Geothermal energy, with an abundant reserve below the subsurface, significantly contributes to achieving green, clean, and sustainable energy supplies [1, 2, 3, 4, 5]. Challenges in exploiting deep geothermal energy arise from insufficient knowledge of the subsurface and the substantial upfront expenses involved in geothermal resource exploration. Operational mines at depths exceeding 1 km are generally located in temperatures high-enough for meaningful heat production conditions, with relatively well characterized geological settings. Consequently, harnessing geothermal energy through the existing infrastructure of deep mines in a safe, efficient and sensible way is a crucial point of attention. [6, 7, 8, 9]. Information from subsurface characterization in existing mines serves as a reference for geothermal extraction and existing shafts and drifts in mining systems substantially reduce the costs associated with geothermal drilling. In addition, the injection of cold water during geothermal system operation cools mining areas through heat exchange, aiding in the management of heat hazards during mining [10, 11].

Geothermal energy in deep mines is currently categorized into two approaches: the use of abandoned mines and the collaborative extraction of geothermal and mineral resources [12]. In the first approach, abandoned mines are typically flooded as drainage measures are no longer maintained after the closure of the mines, and the floodwater can act as an energy medium for geothermal power. Several success stories already exist of utilizing abandoned mines for geothermal energy, such as in Alsdorf, Marienberg, Freiberg in Germany, Limburg in the Netherlands, Folldal in Norway, Asturias in Spain, Glasgow in the UK, and Kingston and Scranton in Pennsylvania, USA [13, 14, 15]. The depths of these geothermal systems generally fall below 200 m, and reservoir water temperatures usually range from 10 to 25 ℃, providing heat supply to nearby buildings. Research on the collaborative extraction of geothermal and mineral resources is less common, but significant progress has been made in China, with successful applications in coal mines such as those in Jiahe, Sanhejian, Zhangshuanglou [6, 16, 17]. These coal mines are mostly deep mines with temperatures exceeding 30°C. Their heat production surpasses that of geothermal mining in shallow abandoned coal mines and the extraction of geothermal energy from mine water successfully reduces the temperature of drifts by 4-6 ℃, effectively mitigating heat hazards in the mines. Within these projects, the primarily extracted geothermal energy involves mine water, with a minor portion from mine return airflow thermal energy. The overarching objective of these deep co-extraction systems is mineral extraction, with geothermal production mainly aimed at managing heat hazards, so that the amount of actually utilizing geothermal energy remains limited.

Unlike the indirect methods of extracting geothermal energy through mine water or airflow, the bedrock harbors a wealth of thermal energy. Direct extraction of geothermal energy from bedrock, facilitated by geothermal systems built within existing deep mines, represents a promising approach for deep mining geothermal exploitation [10, 12]. Although not yet implemented in practice, conceptual models for direct geothermal extraction within deep mines have been proposed. These models serve as a basis for thorough investigations into the system's cooling and heating effects via numerical simulations [7, 18, 19]. However, a current gap in research exists regarding the system's stability. The environment of deep mines and geothermal systems at depths of several kilometers are characterized by elevated temperature (typically over 40°C), high water pressure (typically over 10MPa), and high geostress (typically over 30MPa). Injecting cold fluids in geothermal mining systems expands low-temperature and over-pressurised areas around injection wells, significantly disrupting the original stress field and jeopardizing the system's structural safety and stability [20, 21, 22, 23]. Many studies suggested that stress disturbances in reservoir rocks stem from the combined effects of thermal stress, due to

temperature changes, and poroelastic stress, arising from fluctuations in pore pressure. Decreases in temperature and fluid overpressure can result in reduced effective stress, potentially compromising the stability of surrounding rock [24, 25, 26]. Therefore, conducting coupled THM (thermal-hydraulic-mechanical) studies on the deep mine geothermal extraction system to ensure efficient geothermal production and cooling of the mine drifts, while concurrently maintaining the safety and stability of the mining system, is a challenge that warrants exploration.

Consideration of a wide variety of parameters, including hydraulic, thermal, and mechanical properties, is required for the THM numerical model. In the THM coupling process, complex interactions among physical processes are influenced by the collective influence of numerous parameters. Therefore the construction of a reliable THM geothermal model remains a time-intensive endeavor, Despite advancements in numerical modeling for addressing THM geothermal challenges—for example, the utilization of High-Performance Computing (HPC) to markedly improve computational speed, precision, and the ability to manage large-scale issues[27, 28]—the construction of reliable THM geothermal models remains a daunting task.

Considerable uncertainties in the model development stem from incomplete knowledge of the parameters and the complexity of subsurface structures [29, 30]. Two main aspects contribute to this uncertainty in the technical aspects of geothermal production: subsurface characterization and development options [31]. Understanding of the target reservoir, typically based on data interpretation and empirical correlations, may not fully capture the subsurface property distribution and uncertainty will still remain [32]. Furthermore, the design of the geothermal system often plays a crucial role in influencing reservoir responses, with factors like well spacing, injection rate and temperature being critical considerations in geothermal design [33]. In the deep mine geothermal model examined in this study, the proximity between the geothermal system and the mining system is also investigated.

Enhancing the reliability of geothermal systems necessitates rational parameter selection based on uncertainty analysis and geothermal systems are complex dynamic systems that should be characterized in both space and time [34]. Certain studies focus on uncertainty analysis to explore how various parameters affect the production temperature and stability of geothermal systems under THM coupling conditions. Parameters like the rock's elastic modulus, thermal conductivity, heat capacity, and permeability, along with design elements such as injection rate and temperature, and well spacing, are found to significantly influence the system's response [35, 36, 37, 38]. However, the methodologies employed in these analyses are typically local sensitivity analysis techniques, utilizing partial derivatives or sensitivity coefficients. For instance, the one-at-a-time (OAT) sensitivity analysis approach involves changing one parameter at a time, with others held constant, to determine its impact on the output. OAT provides valuable insights near a baseline point but may not capture the full range of interactions between parameters or model behavior across the entire input space [30]. Global sensitivity analysis, unlike local sensitivity analysis, encompasses the entire range of input parameters, assessing how changes influence model outputs and is more suited to examine nonlinearities and interactions among parameters. Thus, employing global sensitivity analysis in optimising complex deep geothermal systems is a preferable approach [39, 40]. This method entails generating numerous samples through specific sampling strategies within the model parameters' probability distribution, followed by forward simulation of system responses, and then evaluating their impact. Global sensitivity analyses in geothermal systems have so far primarily focused on evaluating, quantifying, and optimizing the production temperature, operational efficiency, and lifespan of the system [41, 42, 43, 44, 45, 46, 47]. Some studies target coupled THM modeling of geothermal production, but investigations into the mechanical stability of the co-mining systems are notably lacking.

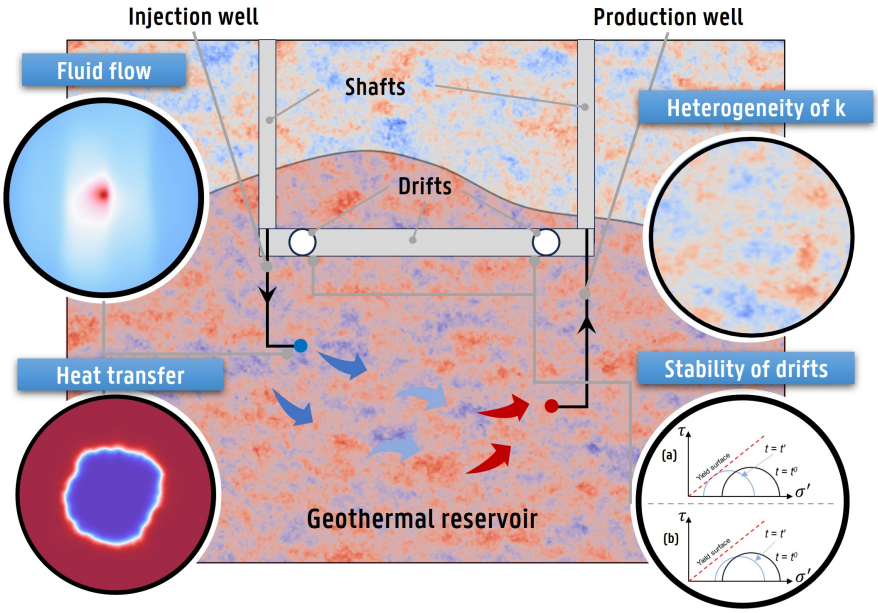

Figure 1: Conceptual representation of geothermal extraction in a deep mine. Top left: fluid flow around the injection well. Bottom left: heat transfer around the injection well. Upper right: heterogeneity of the permeability field. Lower right: the stability evolution of the mining drifts, represented by Mohr-Coulomb circles (a) indicating failure, (b) indicating stability.

This work investigates the cooling effects on the stability of mine drifts, as well as temperature in production wells within the integrated framework of combined mining and geothermal operations. We employ THM (thermal-hydraulic-mechanical) numerical modeling to explore how poroelastic stress and thermal stress influence the stability of mining systems during geothermal operation. A sensitivity analysis using the DGSA (distance-based generalized sensitivity analysis) method is then conducted based on a dataset from 1,000 realizations generated through Latin hypercube sampling. By assigning fixed values to non-sensitive parameters, the system's complexity is reduced, effectively quantifying the uncertainty of sensitive parameters. Lastly, based on the sensitivity analysis results and verification, we outline a framework for system optimization under subsurface uncertainty, guiding effective decision-making for enhanced geothermal energy production and mine stability. Our findings underscore the importance of rational design parameter selection within appropriate geological contexts, facilitating optimal and efficient geothermal operations.

2 Methodology

A 2D thermo-hydro-mechanical finite element model of a synthetic geothermal system situated directly beneath an existing mine is developed (Figure 1), implemented in COMSOL Multiphysics. During the operation of the geothermal system, we analyze the evolution of the temperature and stability changes in the mining system's drifts, as well as the evolution of the production temperature of the geothermal system. Subsequently, the responses of temperature and stability generated from 1,000 stochastic simulations were used as inputs for distance-based generalized sensitivity analysis (DGSA).

2.1 Governing equations

The fluid mass balance equation is written as:

$$\frac{\partial}{\partial t}(\varphi\rho_{\mathrm{f}}) + \nabla\cdot(\rho_{\mathrm{f}}\mathbf{u}) = Q_f \tag{1}$$

where t(s) is time, φ is the porosity, ρ_{f}(kg/m^3)is the density of the pore fluid, $\mathbf{u}$(m/s) is the advective fluid flux, and Q_{f}(kg/m$^3\cdot$s) represents an external source or sink. The storage term of the water mass balance equation can further be expressed as:

$$\frac{\partial}{\partial t}(\varphi\rho_{\mathrm{f}}) = \rho_{\mathrm{f}}\left(\varphi\chi_{\mathrm{f}} + \frac{\partial\varphi}{\partial p_{\mathrm{f}}}\right)\frac{\partial p_{\mathrm{f}}}{\partial t} = \rho_{\mathrm{f}}S\frac{\partial p_{\mathrm{f}}}{\partial t} \tag{2}$$

where χ_{f}(1/Pa) is the fluid compressibility, p_f(Pa) is the fluid pressure, and S(1/Pa) is a storage coefficient, accounting for the compressibility of the porous material and pore fluid. The fluid flux is:

$$\mathbf{u} = -\frac{k}{\mu}(\nabla p_f + \rho\mathbf{g}\nabla d) \tag{3}$$

where k(m^2) is the permeability, μ(Pa$\cdot$s) is the fluid dynamic viscosity, and $\mathbf{g}$(m/s^2) is gravity. d(m) is depth. The external source/sink term Q_{f}(kg/m$^3\cdot$s) is given by:

$$Q_{\mathrm{f}} = -\rho_{\mathrm{f}}\alpha_B\frac{\partial\varepsilon_{\mathrm{vol}}}{\partial t} \tag{4}$$

where α_B is biot coefficient, and the $\varepsilon_{\mathrm{vol}}$ is volumetric strain of the porous matrix.
The energy balance equation is given by:

$$(\rho_{\mathrm{f}}C_{\mathrm{f}})_{\mathrm{eq}}\frac{\partial T}{\partial t} + \rho_{\mathrm{f}}C_{\mathrm{f}}u\cdot\nabla T = \nabla\cdot(\mathbf{q}) + Q \tag{5}$$

where T(K) is temperate, and $(\rho_{\mathrm{f}}C_{\mathrm{f}})_{\mathrm{eq}}$(J/(m$^3\cdot$K)) is the equivalent volumetric heat capacity of porous media:

$$(\rho_{\mathrm{f}}C_{\mathrm{f}})_{\mathrm{eq}} = (1-\varphi)\rho_{\mathrm{s}}C_{\mathrm{s}} + \varphi\rho_{\mathrm{f}}C_{\mathrm{f}} \tag{6}$$

ρ_{s}(kg/m^3) and C_{s}(J/(kg$\cdot$K)) are the density and heat capacity of the solid, and ρ_{f}(kg/m^3) and C_{f}(J/(kg$\cdot$K)) are the density and heat capacity of the fluid, respectively; and Q(W/m^3) is the heat source term, $\mathbf{q}$(W/m^2) is the heat flux:

$$\mathbf{q} = -\lambda_{\mathrm{eq}}\nabla T \tag{7}$$

where, λ_{eq}(W/m$\cdot$K) is the equivalent thermal conductivity of the porous media material, T(K) is temperature. Within porous media, the equivalent parameters are determined by volumetric averaging between the solid phase K_{s} and fluid phase K_{f}:

$$K_{\mathrm{eq}} = (1-\varphi)K_{\mathrm{s}} + \varphi K_{\mathrm{f}} \tag{8}$$

Consequently, the stress tensor $\boldsymbol{\sigma}$ can be expressed through a constitutive equation that encompasses temperature change and fluid pressure change:

$$\boldsymbol{\sigma} = \mathbf{C}(\boldsymbol{\varepsilon} - \boldsymbol{\varepsilon_{th}}) - p_f\mathbf{I} \tag{9}$$

where $\mathbf{C}$ represents the material's elastic matrix, and $\mathbf{I}$ is a unit tensor. The thermal strain ε_{th} is expressed in terms of the coefficient of thermal expansion $\alpha_T(1/\text{K})$ and change from an initial temperature $T - T_{\text{ref}}$:

$$\boldsymbol{\varepsilon_{th}} = \alpha_T(T - T_{ref})\mathbf{I} \tag{10}$$

The relationship between fluid pressure, increment in fluid content ζ, and volumetric strain ε_{vol} is expressed as:

$$p_f = M\left(\zeta - \alpha_B \varepsilon_{vol}\right) \tag{11}$$

where $M(\text{Pa})$ is Biot's modulus, defined as the inverse of the storage coefficient S. The solid deformation complies with force equilibrium:

$$\rho_p \mathbf{g} = -\nabla \cdot \boldsymbol{\sigma} \tag{12}$$

In this study, water properties are assumed to vary with temperature $T(\text{K})$. The impact of temperature on properties such as dynamic viscosity $y_{\text{f}}(\text{Pa} \cdot \text{s})$, heat capacity $\lambda_{\text{f}}(\text{J/kg} \cdot \text{K})$, density $\rho_{\text{f}}(\text{kg/m}^3)$, and thermal conductivity $C_{\text{f}}(\text{W/m} \cdot \text{K})$ was respectively expressed through the following empirical relations [48, 49]:

$$y_{\text{f}} = 1.38 - 0.028T + 1.36 \times 10^{-4}T^2 - 4.64 \times 10^{-7}T^3 + 8.9 \times 10^{-10}T^4 \tag{13}$$

$$\lambda_{\text{f}} = -0.869 + 0.0097T - 1.58 \times 10^{-5}T^2 + 7.98 \times 10^{-9}T^3 \tag{14}$$

$$\rho_{\text{f}} = 838.47 + 1.47T - 0.0037T^2 + 3.72 \times 10^{-7}T^3 \tag{15}$$

$$C_{\text{f}} = 12010.15 - 80.41T + 0.317T^2 - 5.38 \times 10^{-4}T^3 + 3.62 \times 10^{-7}T^4 \tag{16}$$

2.2 Geometry, initial and boundary conditions and model parameters

We develop a 2-dimensional conceptual model of a geothermal system, as depicted in Figure 2. The model includes two mine drifts, each with a 3m radius, situated at a depth of 1,100m and spaced 500m apart. The geothermal injection and production wells are positioned beneath the two drifts, at vertical distances of 120m and 220m from the mine drifts, respectively. The model domain is 3 km wide, centered on the midpoint between the two drifts, with a depth range from 300m to 2,300m.

The surface temperature is set to 10°C and the geothermal gradient to 30°C/km, with the sides featuring thermal insulation. The pressure boundary condition represents an initial hydrostatic gradient of 10 MPa/km, setting the top boundary at 3MPa and the bottom at 23MPa, and no-flow conditions to the sides. Vertical self-weight stress is applied to the top, and roller support conditions are employed on the remaining three sides. Gravity influences both pressure and effective stress within the model, and stress equilibrium is established prior to the operation of the geothermal system.

Comparing isothermal and non-isothermal injection is a typical approach for analyzing thermal stress effects in THM models [50, 51]. In this work, to accurately study the impact of thermal stress and poroelastic stress on the system we establish two scenarios: i) isothermal injection (with both domain and injection water temperature of 30℃) and ii) non-isothermal injection (with an injection water temperature of 10℃ and domain temperature following the geothermal gradient).

To consider spatial heterogeneity, we generate permeability, porosity, and Young's modulus fields through sequential Gaussian simulation, with a range of 100m for the variogram in the flow direction and a primary direction set at 60° [43, 52]. The triangular mesh used in this study contains about 24,000 elements in each model. The parameters of the system and material properties utilized in the simulation are summarized in Table 1 [25, 53, 51, 54, 50, 55]:

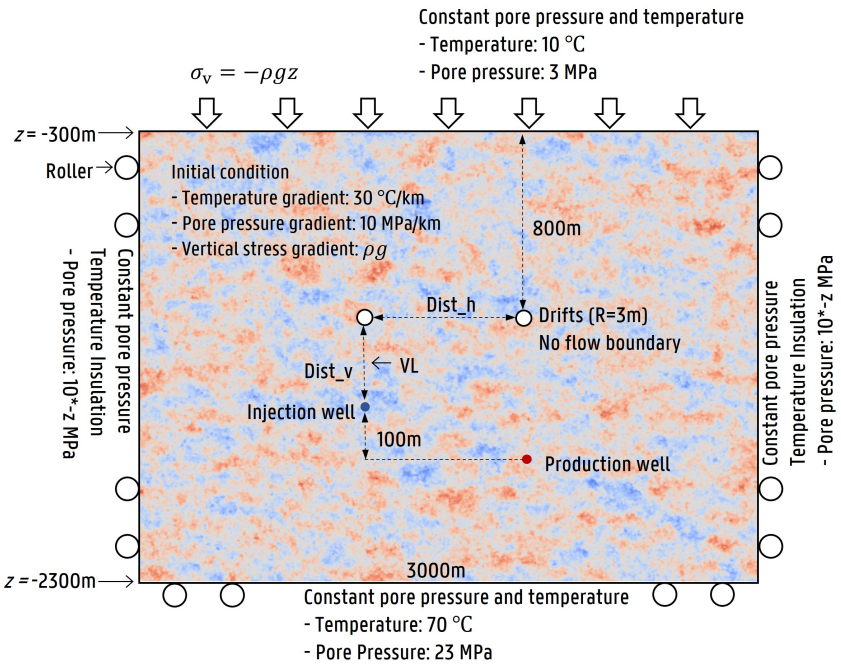

Figure 2: Schematic of heterogeneous 2-D numerical model including initial and boundary conditions (not to scale). In the isothermal injection scenario in Section 2 and model scenarios in Section 3, the initial condition of temperature is set to 30 °C, with both the top and bottom temperatures at 30 °C, disregarding the temperature gradient.

2.3 Mine stability assessment

The mobilized friction angle ϕ is used to assess the stability of the rock mass [50, 51]. Assuming a Mohr-Coulomb failure criterion, the mobilized friction angle is given by:

$$\phi = \tan^{-1}\left(\frac{\sigma}{\sigma_n'}\right) \tag{17}$$

where σ is the deviatoric stress and σ_n' is the effective normal stress. A point of the rock mass is deemed stable when ϕ is lower than the friction angle 30°.

2.4 Stochastic analysis

Given the limited knowledge of the subsurface, we explore the uncertainty of model parameters through stochastic simulation. Recognizing the inherent limitations in accurately determining all model parameters, we extend our analysis to encompass a broader spectrum of possible outcomes. This is achieved by assigning uniform distributions to 14 critical parameters, which include 4 design parameters, 8 material properties, and 2 heterogeneity parameters while keeping the remaining variables constant. To systematically investigate the impact of these uncertainties, we employ the Latin Hypercube Sampling (LHS) method to generate 1,000 realizations of the model parameters[56]. These realizations enable us to conduct a series of forward simulations that reflect a wide range of potential conditions. For these realizations the geothermal gradient, is also incorporated. The surface temperature is set at 10°C and the gradient at 30°C/km. The specified range for each parameter is detailed in Table 1.

Type	Parameters	Unit	Iso/Non-Iso Simulations	Stochastic Simulations	Abbreviation
Heterogeneity parameters	Range	m	100	U[20 200]	Range
	Orientation	°	60	U[60 120]	Angle
Design parameters	Well spacing	m	500	U[200 800]	Dist_h
	Vertical distance from the drift to the well	m	120	U[50 200]	Dist_v
	Temperature of injected water	°C	10, 30	U[10 30]	T_inj
	Pumping rate	kg/s	50	U[20 70]	P_rate
Material properties	Mean of $log_{10}K$	m^2	-13	U[-14 -12]	K_mean
	Variance of $log_{10}K$	m^2	0.5	U[0.1 1]	K_var
	Porosity	1	0.125	U[0.05 0.2]	Porosity
	Young's modulus	GPa	15	U[10 20]	Y_modu
	Density	kg/m^3	2500	U[2300 2700]	Dens
	Thermal expansion	1/K	5e-6	U[1e-6 1e-5]	T_expa
	Heat capacity	J/kgK	1050	U[800 1300]	H_capa
	Thermal conductivity	W/mK	1.85	U[1.2 2.5]	T_cond

Table 1: Geological and design parameters and material properties used in the numerical model.

2.5 Distance-based Generalized Sensitivity Analysis (DGSA)

This work employs Distance-based Generalized Sensitivity Analysis (DGSA) to analyze the sensitivity of the selected model parameters to the reservoir response simulated by the stochastic simulation. DGSA is capable of handling single outputs, as well as more complex time-dependent or spatiotemporal outputs [57, 39, 40]. A distinctive feature of DGSA is its use of clustering algorithms to categorize output variables into different groups based on their mutual distances, thereby facilitating the assessment of uncertainty.

Initially, this method divides outputs into several clusters using a distance-based clustering approach, examining the cumulative distribution function (CDF) of a specific parameter in each cluster and comparing it to the original distribution. This process yields the normalized sensitivity index by considering the average differences between the CDFs in each cluster. DGSA employs a resampling technique to quantify variations among samples redistributed within clusters. Sensitivity is represented by the average of the mean differences across all categories, if distributions within various categories differ significantly, the parameter is deemed sensitive. In this study, parameters are defined as sensitive if their sensitivity value exceeds 1 [58].

$$S(X) = \frac{1}{C}\sum_{c=1}^{C} \hat{d}_{c,s}, \text{ with } \frac{\hat{d}_c}{\check{d}_a^c} \tag{18}$$

$$\hat{d}_{c,i} = d_{L1}F(X), F(X|c), c = 1, \ldots, C \tag{19}$$

where $\hat{d}_{c,s}$ is the normalized distance within a cluster, $\hat{d}_c$ is the average of the distances for cluster c, and $\check{d}_a^c$ is the a_{th} quantile of the distances within cluster c, with a being set to 0.95, and $\hat{d}_{c,i}$ is the $L1$ distance between the cumulative distribution function of the entire dataset $F(X)$ and the cumulative

distribution function of the dataset conditioned on cluster c, $F(X|c)$.
In similar context, it is possible to determine a conditional effect (i.e. interaction between parameters). This approach delineates the impact of one parameter when it is conditioned upon the level (or grouping) of a different parameter. The method for deriving the second-order conditional effect adheres to a methodology comparable to the previous one, expressed as follows:

$$S(X_i|X_j) = \frac{1}{C}\frac{1}{L}\sum_{c=1}^{C}\sum_{l=1}^{L}\hat{d}_{c,i|j},l^S \text{ with } \hat{d}_{c,i|j},l^S = \frac{\hat{d}_{c,i|j,l}}{\hat{\hat{d}}_{c,i|j,l}(a)}, i,j = 1,\ldots,k; l = 1,\ldots,L; c = 1,\ldots,C \tag{20}$$

Here, the term $\hat{d}_{c,i|j,l}$ is the normalized $L1$ norm distance that accounts for the disparity between the distribution of X_i in class C and the distribution where X_j is at a specific level l.
In this study, the number of clusters is preset to 3, categorizing responses into "good," "moderate," and "poor" to assess the model's performance. As an unsupervised method, the clustering approach involves defining response labels based on a subjective interpretation of the expected response. Smaller changes in stability are considered "good" when evaluating the stability of drifts, while faster cooling is considered "good" for the temperature of drifts. The DGSA method contributes to parameter optimization in the model in two ways. First, by analyzing the distribution of the CDFs of the sensitive parameters across the 3 groups to inform model design, aiming to align sensitive parameters' probabilities with the "good" label. Second, by fixing values of insensitive parameters at the average of the initial value range, which reduces the uncertainty of the system responses and assists in model calibration and optimization.

3 THM modeling results

Simulations of 30-years geothermal operation and associated geomechanical reservoir response are conducted for both isothermal injection (30°C) and non-isothermal injection (10°C), temperature of injected water in the latter being below the initial in-situ temperature. This study focuses on the effects of the injection well on the left drift, particularly on the vertical line (VL) between the injection well and the drift lower edge.

3.1 Coupling between pressure and temperature

In the THM geothermal model, pressure changes migrate rapidly, with more pronounced pressure changes around the injection well that gradually diffuse towards the drift edge. Conversely, the area of temperature disturbance expands more slowly. As illustrated in Figure3, under isothermal injection conditions, the temperature along the VL remains constant, and the pressure change stabilizes within a very short duration (0.1 years), with greater pressure values closer to the injection well. Under non-isothermal injection conditions, as shown in Figure4, temperature disturbance migrates slowly with the same maximum temperature drop (-20°C) controlled by the injection temperature. The decrease in temperature caused by the propagation of the cold front leads to a notable increase in pressure. After 30 years of operation the the Δp near the injection well caused by isothermal injection approximates 0.22MPa, while after non-isothermal injection, it reaches 0.75MPa. In the region near the drift, the pressure change rises from 0.16MPa to 0.21MPa, marking a 31% increase. This occurs because in areas affected by temperature drop, the decrease in fluid temperature leads to an increase in dynamic viscosity, which impedes fluid flow and leads to increased pressure in that area, thus

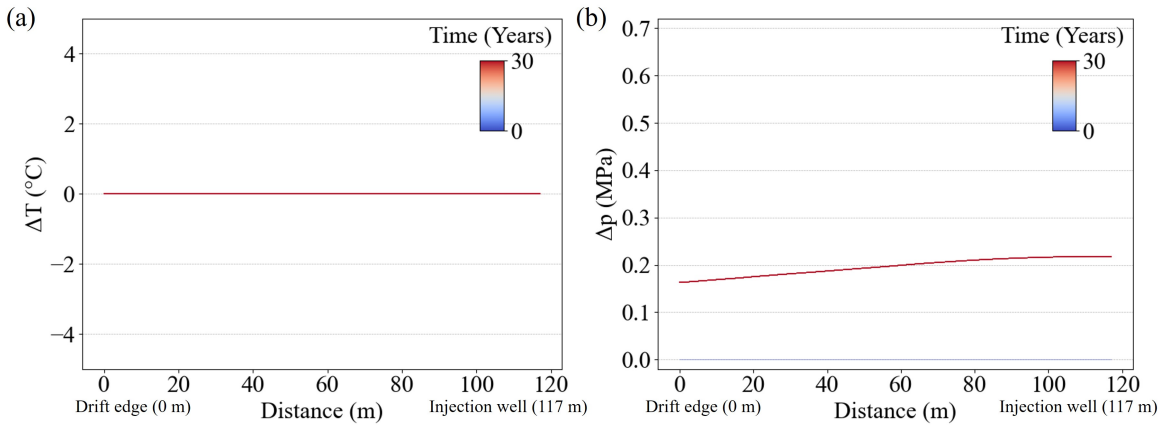

Figure 3: Spatiotemporal evolution of ΔT and Δp on the measurement line VL during isothermal injection: (a)ΔT, (b)Δp.

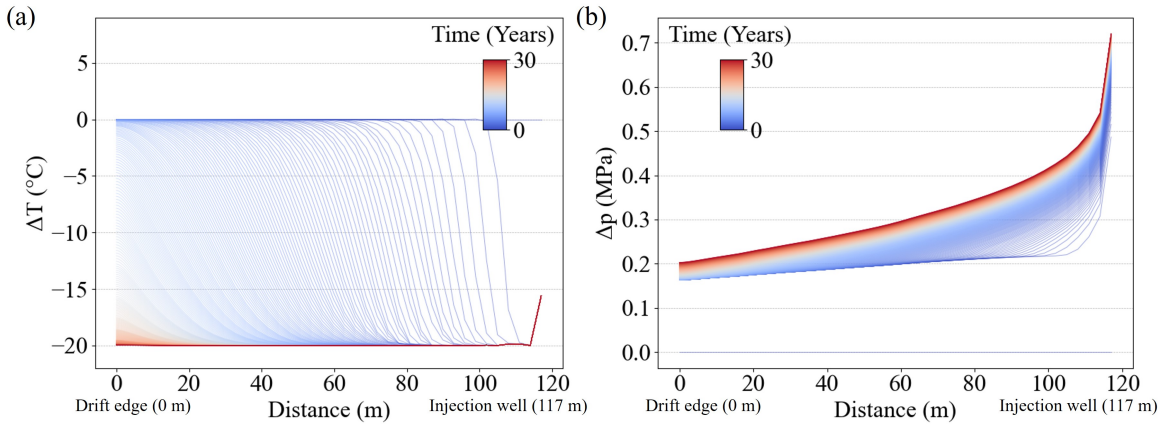

Figure 4: Spatiotemporal evolution of ΔT and Δp on the measurement line VL during non-isothermal injection: (a)ΔT, (b)Δp.

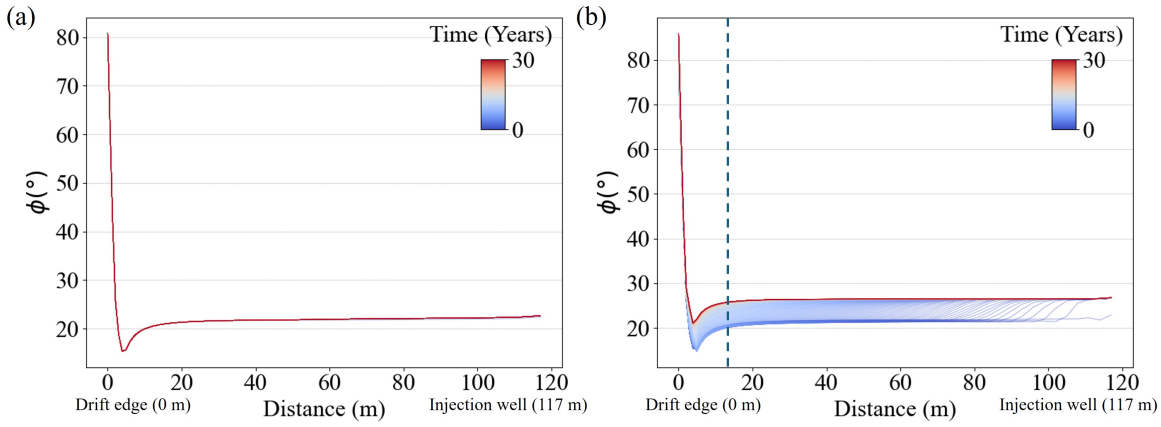

Figure 5: Spatiotemporal evolution of ϕ on the measurement line VL stability: (a) isothermal injection, (b) non-isothermal injection.

potentially increasing the risk of instability. In non-isothermal injection, the mechanical response is not solely the result of pressure or temperature acting independently, but rather a combined effect of rapidly developing pressure front first, followed by the thermal effect on cooling areas, and the pressure changes in these cooling areas during the process.

3.2 Evolution of the poroelastic and thermal stress fields

The response characteristics of poroelastic stress and thermal stress reflect those of pressure and temperature migration, with both factors adversely affecting the stability of the surrounding rock. An increase in pore pressure reduces the effective stress in the rock, leading to an increase in the mobilized friction angle, denoted as an increase in ϕ, and a heightened likelihood of rock failure. Injection of cold water decreases thermal stress in the rock, thereby increasing the risk of failure in the surrounding rock and consequently weakening the stability of the mine drifts [24, 59].

Due to the excavation, a pronounced stress concentration is observed within approximately 5r (15m) of the drift[60]. At the drift's edge, initial ϕ can reach 80°, with certain areas exhibiting low ϕ due to changes in the maximum and minimum principal stresses (Figure 5a). A comparison of the impacts of isothermal and non-isothermal injection on ϕ demonstrates that temperature significantly influences system stability more than pressure does and the variation in ϕ values mirrors the characteristics of temperature propagation, as shown in Figure5. In the area distant from the drift, as indicated by the dashed line on the right side of Figure5(b), ϕ typically ranges from 21° to 26°. However, at the dashed line's left, the initial ϕ values are significantly affected by the excavation. Considering this study is conducted on the foundation of an existing mine system for geothermal operation, we posit that stability on the left side of the dashed line is controlled by excavation, assuming the stress concentration area around the drift remains safe due to support. Conversely, the right side is affected by geothermal operation, and if the ϕ on this side exceeds 30° during geothermal operation, failure is reached. We designate the position 5r (15m) below the drift as a potential risk point for monitoring the mechanical response during system operation. Specifically, in the area between the drift and the injection well, a pattern of ϕ initially decreasing and then increasing suggests that while the surrounding rock's stability is finally weakened, there is an improvement in stability at the early stage.

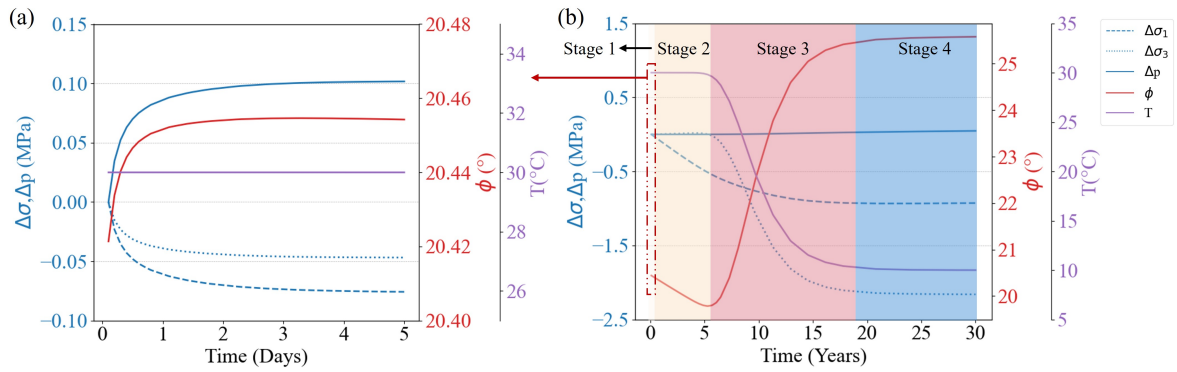

Figure 6: Effective stress, pressure, stability, and temperature changes at potential risk points: (a) 5-day injection, (b) 30-year injection.

3.3 Evolution of the mine stability at the potential risk points

During simulation of the 30-year geothermal operation, we examine the $\Delta\sigma_1$, $\Delta\sigma_3$, Δp, ϕ, and ΔT at the potential risk point(5r (15m) below the drift) to evaluate the evolution of stability. The changes in stability at the risk point can be divided into four distinct stages (Figure6):

1) Slight Reduction (0-5 days): Figure6(a) reveals that 5 days post-injection, a short-term decrease in both σ_1 and σ_3, caused by the rapid migration of injection-induced pressure and an increase in pore pressure, leads to reduced stability.

2) Minor Enhancement(0-6 years): In this phase, the temperature remains relatively unchanged; due to the increase in thermal stress around the injection well, the potential risk point's σ_1 decreases, but σ_3 experiences a slight increase due to the effect of the stress arching. Therefore ϕ decreases by about 0.6, indicating an improvement in stability.

3) Transition(6-19 years): As the temperature of this point begins to decrease, influenced by thermal stress, bothσ_1 and σ_3 decrease, indicating significant reduction in the stability.

4) Deterioration(19-30 years): The temperature and mobilized friction angle stabilize, as the area becomes completely encompassed by the spread of the cold plume.

It should be noted that although the observed behavior is informative on the processes taking place and can thus be generalized, they remain characteristic of one set of subsurface properties and design parameters, especially in terms of absolute values. It is crucial to consider all potential risks more systematically and quantitatively.

4 Uncertainty quantification results

4.1 Sensitivity analysis

As previously mentioned, 3 clusters were defined in this study, categorizing responses into 'good,' 'moderate,' and 'poor' clusters by the K-medoids clustering method. Figure7 displays the clustering results of the 1,000 realizations. For the drift stability, the group with small ϕ values is categorized as "good" (blue). For the temperature at the drift, the group exhibiting fast temperature drop is deemed "good". Whereas for the production well temperature, the group with slow temperature decrease is classified as "good". Figure8 illustrates the CDF distributions of the 5 parameters showing the most significant distribution differences across the responses. Based on Figure8, the sensitivity of each parameter across the 3 groups is quantified, defining parameters with a sensitivity value over 1 as

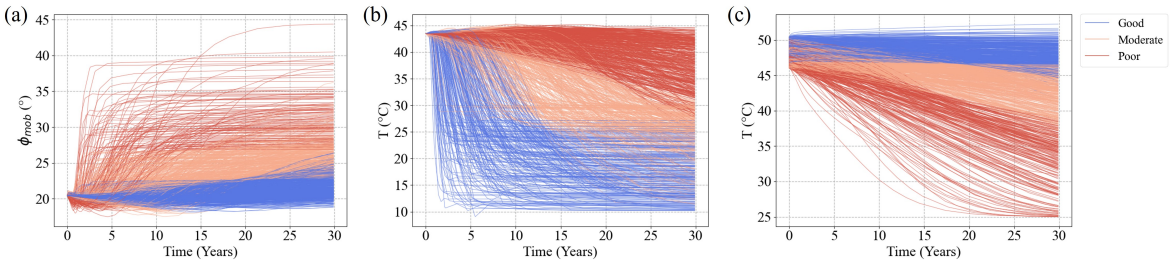

Figure 7: Clustering results of response: (a) stability of the drift, (b) temperature at the drift, (c) temperature at the production well.

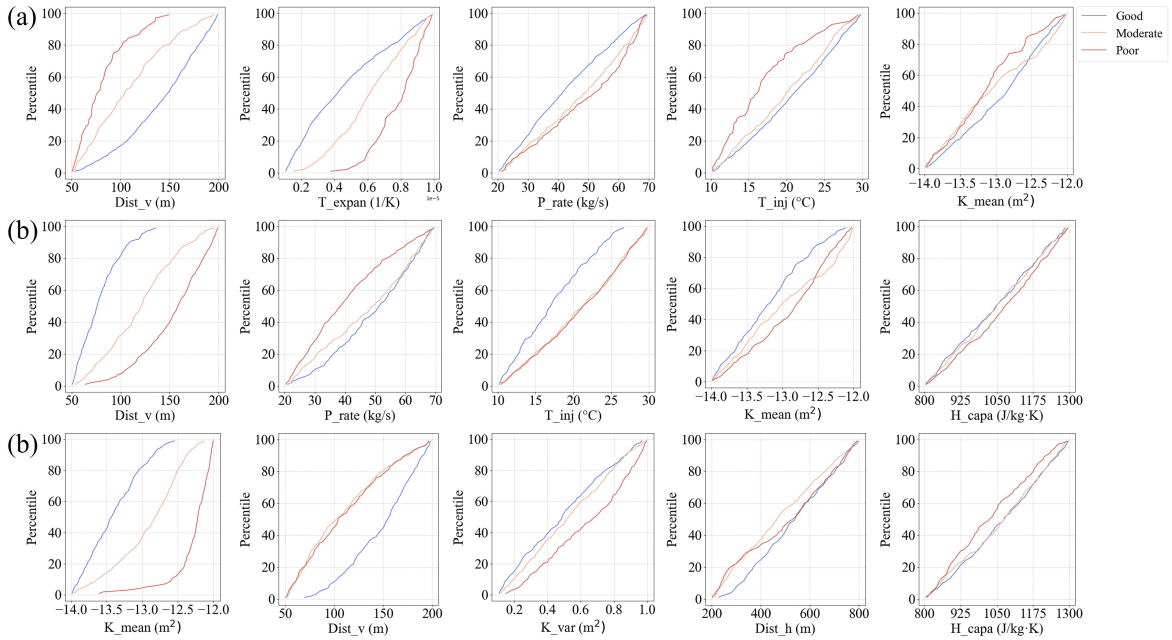

Figure 8: CDF distribution of top 5 parameters with greatest variance in responses across 3 clustering groups: (a) stability of the drift, (b) temperature at the drift, (c) temperature at the production well.

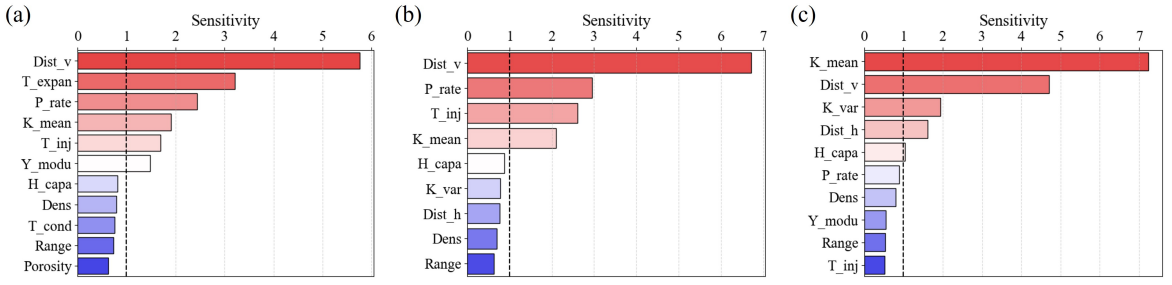

Figure 9: Sensitivity analysis results of responses (including all sensitive parameters and top 5 insensitive parameters): (a) stability of the drift, (b) temperature at the drift, (c) temperature at the production well.

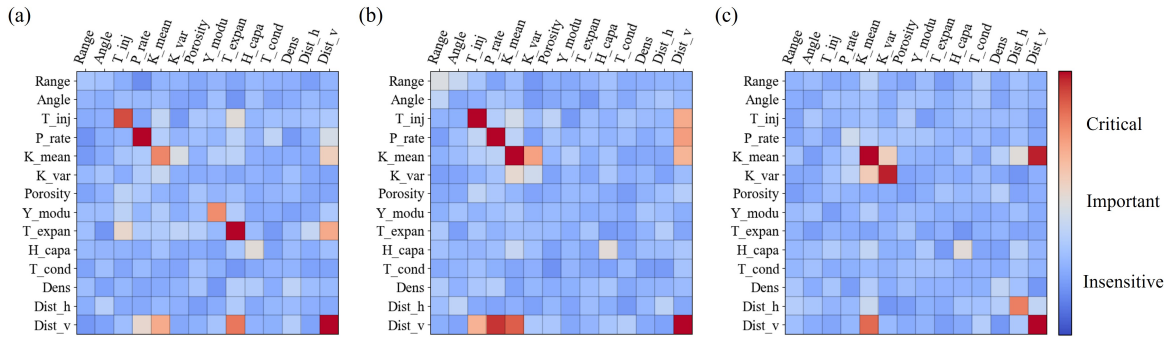

Figure 10: Outcomes of inter-parameter sensitivity values: (a) stability of the drift, (b) temperature at the drift, (c) temperature at the production well.

sensitive.

For the stability analysis of the drift, Figure 9(a) identifies the vertical distance between the injection well and the drift as the most sensitive parameter. This is followed by thermal expansion coefficient, injection rate and temperature, and permeability. Figure8(a) indicates that an increased vertical distance correlates with enhanced safety of the drift. In the "poor" category, about 78% of the realizations feature a vertical distance of less than 100 m, The remaining 22% are located at 100-150 m, whereas in the "good" category, realizations with a vertical distance exceeding 100 m constitute 83% of the group, when the distance exceeds 150 m, samples categorized as "poor" no longer appear. Within the vertical distance range, the influence of pore pressure is minimal, suggesting that thermal stress more significantly impacts the stability of the drift compared to poroelastic stress, a conclusion further supported by the high sensitivity of the thermal expansion coefficient. Figure8(a) shows that a higher thermal expansion coefficient associates with an increased risk. In the "poor" category, most realizations display high ϕ values towards the end of the simulation, albeit with a slight improvement at the early stage. Parameters related to fluid injection suggest that a higher injection rate, lower permeability, and lower injection temperature (resulting in a larger temperature difference) contribute to unfavorable stability evolution in the drift.

SA results for the temperature of the drift, as shown in Figure9(b), reveal that the vertical distance between the drift and the well is the primary parameter influencing cooling. Unlike the results for stability, a smaller vertical distance is favorable for cooling. Injection rate and permeability are additional sensitive parameters, with their CDF (Figure8) results indicating a more pronounced impact on the "poor" category.

In the SA results for the production well temperature, as illustrated in Figure9(c), Permeability emerges as the most sensitive parameter in geothermal systems. Increased permeability facilitates earlier thermal breakthrough, characterized by a significant reduction in production temperature, which can be defined as a 10% decrease in the difference between the initial production temperature and the injection temperature. Additionally, both the vertical distance between the well and the drift and the well spacing are sensitive, particularly the vertical distance. In this model, a greater vertical distance indicates increased depth, consistent with the conventional notion that deeper geothermal systems are more efficient [3]. The well spacing significantly affects the likelihood of thermal breakthrough, with a smaller horizontal distance increasing the probability of occurrence. However, during the 30-year simulation period, most realizations did not exhibit thermal breakthrough. It is anticipated that with extended extraction duration or high rates, the sensitivity of well spacing to production temperature will increase.

The sensitivity analysis (SA) presented in Figure10 uncovers intricate interactions among the system's parameters, particularly emphasising the pivotal role of the vertical distance between the mine drift and the geothermal system. For the drift's response, vertical distance, in conjunction with mean permeability, injection rate, predominantly influences reservoir behavior. As to the temperature at the production well, the mean and variance of permeability exhibit significant interaction, indicating that the spatial distribution has an impact on water propagation. A notable interaction between well spacing and permeability emerges, similar to previous studies only focusing on geothermal heat production [31, 61]. These interactions all relate to how fast the temperature front migrates to the drift or the production well. Furthermore, in terms of the stability of the drift, vertical distance and thermal expansion exhibit significant interplay, aligning with our prior findings that the stability of the drift is governed by the thermal stress.

In summary, vertical distance and permeability emerge as the most sensitive parameters among the three responses, each showing diverse distribution trends in the "good" category. Crucial design parameters of the model (including pumping rate, injection temperature, and well spacing) and some material properties (including the permeability, thermal expansion coefficient, Young's modulus, and heat capacity) prove particularly sensitive. Other material properties, such as the porosity, thermal conductivity, density, range, and angle do not show significant sensitivity in the responses nor interactions, therefore, we recommend maintaining these five parameters at the average of their prior value ranges.

By reducing the model's complexity and uncertainty via the DGSA method, we can utilize the results to refine and limit the range of sensitive parameters, enhancing the probability of achieving desired performance of the system.

4.2 Suggestions to decision-making

Type	**Parameters**	**Prior Values**	**Suggested Values**
Design parameters	Well spacing(m)	U[200 800]	U[345 745]
	Vertical distance from the drift to the well(m)	U[50 200]	U[109 117]
	Temperature of injected water(°C)	U[10 30]	U[17 22]
	Pumping rate(kg/s)	U[20 70]	U[38 47]
Material Properties	Mean of $log_{10}K$ (m^2)	U[-14 -12]	U[-13.1 -12.8]
	Variance of $log_{10}K$ (m^2)	U[0.1 1]	U[0.16 0.6]
	Young's modulus(GPa)	U[10 20]	U[11.4 16.7]
	Thermal expansion(1/K)	U[1e-6 10e-6]	U[1.5e-6 2.9e-6]
	Heat capacity(J/kgK)	U[800 1300]	U[1015 1235]

Table 2: Prior model parameters and optimal value used for verification.

This section introduces an analytical model based on the DGSA results, aimed at identifying the optimal range for sensitive parameters. This approach involves determining a parameter range by evaluating the probability density of sensitive parameters, that leads to desired performance and thereby enhancing the likelihood of achieving responses categorized as "good" during the DGSA clustering in forward simulations.

For parameters that appear only once across the three sensitivity analyses, a single probability density is evaluated. For parameters appearing multiple times, we employ a statistical overlap analysis method, which identifies common areas between different groups by analyzing the overlap of probability densities, akin to the concept of Pareto optimality. A range is defined that effectively balances the probability distributions among each group. By setting a threshold of 90% of the peak value on the

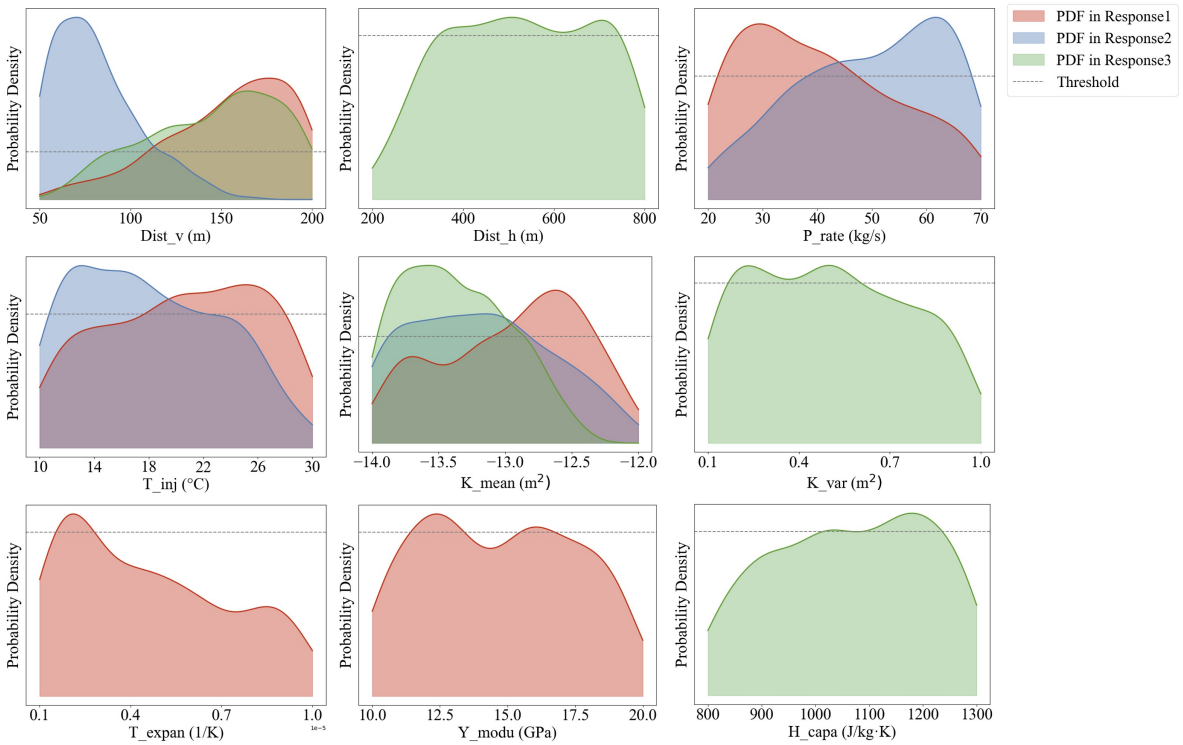

Figure 11: Parameter optimization process: Red, blue, and green represent the probability density functions for parameters of samples labeled as "good" for response1 (stability of the drift), response2 (temperature at the drift), and response3 (temperature at the production well), respectively.

overlap probability density, the optimal parameter value range is calculated. A range exceeding this threshold indicates a high likelihood of the parameter satisfying the criteria in one or all groups, thus representing the optimal parameter distribution range.

Using the vertical distance as an example (see Figure11), this parameter shows varying distribution trends in the "good" category for different responses. For stability of the drift and temperature at the production well, larger values are favored, with the most concentrated distribution observed at 180m. Conversely, for cooling of the drift, smaller values are desirable, with approximately 70m identified as the optimal range for cooling. According to this method, the peak of the probability distribution across the three categories occurs around 112m, establishing the optimized range as 109m to 117m. While this method may not always yield the optimal expected response when optimizing parameters with diverse distributions, it effectively mitigates the likelihood of poor-case scenarios in the system response.

The recommendations for optimized sensitive design parameters and the favorable material parameters are provided in Table2. These results demonstrate that for informed decision-making for the development of geothermal systems beneath deep mines, the suggested design parameter ranges can significantly enhance the system's performance. This applies in particular for geological layers where the material properties, specifically permeability, Young's modulus, thermal expansion coefficient, and heat capacity, align with Table2.

4.3 Verification of the suggestions

In the preceding chapter, we determined the optimal design parameters of the system and ranges of material parameters ranges to perform optimally. Building on this, we generate 200 new realizations

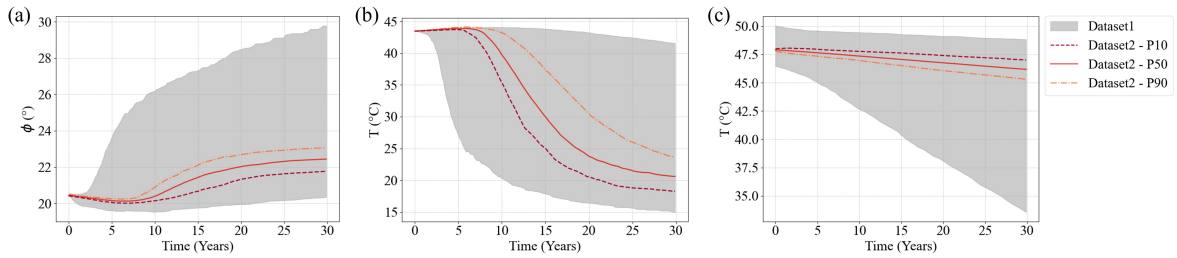

Figure 12: P10, P90 ranges on dataset1(before optimization) and P10, P50, P90 curves on dataset2(after optimization): (a) stability of the drift, (b) temperature at the drift, (c) temperature at the production well.

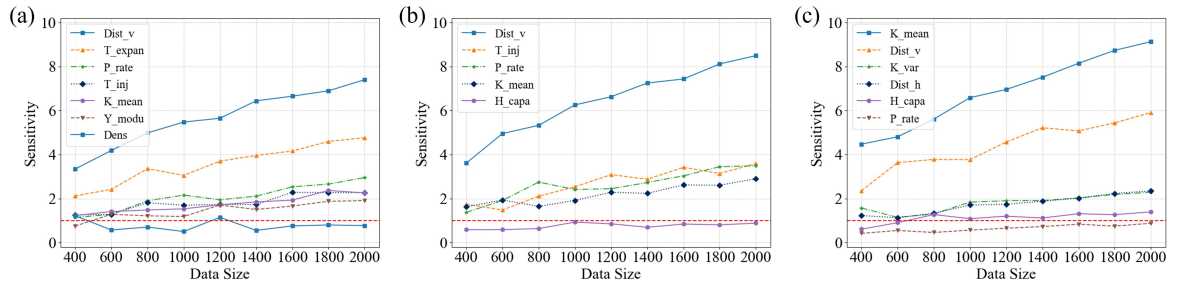

Figure 13: Impact of sample size on DGSA result analysis: (a) stability of the drift, (b) temperature at the drift, (c) temperature at the production well.

using the Latin hypercube sampling method to sample from the optimal parameter ranges and compare their responses with earlier results to validate the feasibility of this approach. For every group of responses, both prior to and following optimization, we compute the P10, P50 and P90 curves across the entire time series, and compare the distribution ranges to validate the optimal parameter selection. The results of post-optimization response demonstrate a significant reduction of uncertainty in the stability of the drift, compared to the initial range. In Figure12(a), the maximum ϕ in P90 curve is merely 22.8°, in contrast to 29.6° in the initial range, indicating a considerable improvement in stability, and no failure occurring in any realization. Simultaneously, the cooling effect of the drift is optimized, resulting in a more focused distribution. Within approximately 15 years, half of the realizations attain at least a temperature reduction of 13°C. As previously mentioned, when searching for optimal parameters in probability curves with divergent distribution trends, it is not possible to achieve the best outcomes simultaneously for both responses. However, the optimized parameter range effectively avoids poor scenarios where the drift either suffers damage or fails to cool down, making the optimization highly effective.

The temperature at the production well also exhibits a highly desirable distribution. None of the 200 realizations exhibit signs of thermal breakthrough after 30 years of system operation. These observations all suggest that the optimization of model parameters is both feasible and effective. Note that since the optimum design parameters were selected based on the full parameter range, we expect to avoid "poor" behavior also for less favorable subsurface parameter combinations, although in that case the risk would increase.

4.4 Sample size of the DGSA

The sample size significantly influences the results of the DGSA [39, 43]. To ensure optimal results using the smallest possible sample size, we utilized a 5-fold cross-verification technique, assessing the DGSA results in multiple scenarios with sample sizes ranging from 400 to 2,000.

Our analysis indicates that for the stability of the drift, when the sample size reaches 600, the least sensitive parameter, Young's modulus, becomes sensitive. With smaller sample sizes, the influence of Young's modulus on the mechanical response might be neglected. Similarly, the heat capacity appears non-sensitive for the temperature of the production well until the sample size increases to 800. This shift further highlights the critical role of sample size in identifying key sensitive parameters. Sensitivity of other parameters remain unchanged across all sample sizes. Furthermore, the hierarchy of parameter sensitivity remains consistent with the outcomes observed in large samples, underscoring the DGSA method's effectiveness even with limited sample size. This approach proves adequate for discerning the sensitivity of crucial parameters, as evidenced by our temperature analysis of the drift, wherein all sensitive parameters display sensitivity from the smallest sample size evaluated.

Considering these findings, we recommend a sample size of 800 for DGSA analysis in the context of this study, as this size not only provides faithful sensitivity evaluation for all major parameters but also ensures the stability and reliability of the analysis outcomes in a computationally efficient manner.

5 Discussion

This study investigates the feasibility and optimized design strategies for geothermal operation in deep mine systems. While previous research has focused on the design concept and heat production performance of such systems, a thorough assessment of system stability remained unexplored. Nevertheless, it is of considerable research importance to address the challenge of practically optimizing the integrated system with safe mining operations, rapid drift cooling, and efficient geothermal energy production.

Our research highlights the significant influence of design parameters and material properties on the performance of the geothermal system; it identifies optimal system design, with especially the distance between the geothermal system and the mine system as a critical factor. The investigation reveals the trade-off between the stability of the drift and its cooling effect, highlighting the importance of selecting an appropriate vertical distance to balance these factors. Previous studies have focused on the impact of rock properties on geothermal system efficiency [62, 63], our work presents similar findings through alternate methodologies, Permeability is considered the most critical rock property in our system. It is noteworthy that our study encompasses a wide range of extreme scenarios. There is no correlation between porosity and permeability in our research. However, in real-world scenarios, these parameters can exhibit a correlated relationship, affecting the efficiency and stability of geothermal operations. Thus, it is worth considering in more realistic geological contexts. In summary, we demonstrate that by selecting a rational set of design parameters under appropriate geological settings, efficient geothermal operation in deep mines can be realized. The applicability of our methods extends to more ambitious endeavors such as enhanced geothermal systems or CO_2 sequestration projects, where reservoir stability is critically affected by the stress alterations from injection processes, raising the risk of seismic events [64, 65, 55, 66]. Therefore, such systems should pay more attention to the evolution of reservoir stability, and deeper projects will incur higher investment costs. The design optimization strategy introduced here, guided by the coupled THM model analysis, and the DGSA offers valuable insights for decision-making in such advanced applications.

It was shown that DGSA allows the identification of optimum parameter ranges prior to performing any costly field investigations or investments. The next logical step is to update Uncertainty Quantification once additional data become available, being either field experiments to better characterize subsurface parameters or early production data. In such a context, Bayesian Evidential Learning (BEL) would constitute an effective strategy. BEL bypasses complex model inversion or data assimilation by directly predicting target variables from data through machine learning and it genuinely complements DGSA by sharing the same prior simulations [43]. BEL would therefore be adapted to be applied in the context of deep mine stability, as already effectively demonstrated in previous research [41, 67, 68, 52, 69, 70].

6 Conclusions

This work investigates the potential of geothermal energy production beneath existing deep mines, providing insights for enhancing geothermal project design. Utilizing the thermo-hydro-mechanical geothermal model, we assess the effects of cold water injection on the geothermal system's long-term mechanical stability and the temperature distribution within the mine drifts. Additionally, the Distance-based Global Sensitivity Analysis (DGSA) method is implemented to evaluate the sensitivity of model parameters, offering direction for model optimization. The findings of our analysis are summarized as follows:

1. Thermal stress significantly impacts the stability of drifts during cold water injection, with poroelastic stress being predominant at the onset of geothermal operation. These stresses lead to a decrease in stability, despite a temporary increase in stability at the base of the drift at the initial stages of the operation.

2. The relative location of the geothermal and mining systems is crucial for achieving satisfactory performance of the systems. Injection rate and temperature, along with rock properties such as thermal expansion coefficient, permeability, Young's modulus, and heat capacity, are critical in dictating the system's behavior.

3. The application of the DGSA method for parameter optimization proves to be effective in significantly enhancing system performance.

4. For the DGSA analysis involving 14 parameters, a sample size of 800 is identified as optimal, balancing comprehensive parameter sensitivity identification and computational efficiency.

This study's insights into parameter sensitivity significantly enhance the design and optimization of subsurface models, particularly for geothermal energy applications. Our findings could lead to safer, more sustainable subsurface renewable energy operations.

References

[1] Austin Anderson and Behnaz Rezaie. Geothermal technology: Trends and potential role in a sustainable future. *Applied Energy*, 248:18–34, 2019.

[2] Xianzhi Song, Yu Shi, Gensheng Li, Ruiyue Yang, Gaosheng Wang, Rui Zheng, Jiacheng Li, and Zehao Lyu. Numerical simulation of heat extraction performance in enhanced geothermal system with multilateral wells. *Applied energy*, 218:325–337, 2018.

[3] William E Glassley. *Geothermal energy: renewable energy and the environment*. CRC press, 2014.

[4] Arman Aghahosseini and Christian Breyer. From hot rock to useful energy: A global estimate of enhanced geothermal systems potential. *Applied Energy*, 279:115769, 2020.

[5] Jon Limberger, Thijs Boxem, Maarten Pluymaekers, David Bruhn, Adele Manzella, Philippe Calcagno, Fred Beekman, Sierd Cloetingh, and Jan-Diederik van Wees. Geothermal energy in deep aquifers: A global assessment of the resource base for direct heat utilization. *Renewable and Sustainable Energy Reviews*, 82:961–975, 2018.

[6] Pingye Guo, Manchao He, Liange Zheng, and Na Zhang. A geothermal recycling system for cooling and heating in deep mines. *Applied Thermal Engineering*, 116:833–839, 2017.

[7] Yonghui Huang, Yanlong Kong, Yuanzhi Cheng, Chuanqing Zhu, Jixiong Zhang, and Jiyang Wang. Evaluating the long-term sustainability of geothermal energy utilization from deep coal mines. *Geothermics*, 107:102584, 2023.

[8] Javier Menéndez, Almudena Ordóñez, Rodrigo Álvarez, and Jorge Loredo. Energy from closed mines: Underground energy storage and geothermal applications. *Renewable and Sustainable Energy Reviews*, 108:498–512, 2019.

[9] Josiane Jello and Tugce Baser. Utilization of existing hydrocarbon wells for geothermal system development: A review. *Applied Energy*, 348:121456, 2023.

[10] Mei-feng CAI, Ming-hui MA, Ji-liang PAN, Xun XI, and Qi-feng GUO. Co-mining of mineral and geothermal resources: a state-of-the-art review and future perspectives. *Chinese Journal of Engineering*, 44(10):1669–1681, 2022.

[11] Ping-ye GUO, Mo-hua BU, Peng ZHANG, and Man-chao HE. Research progress on the prevention and utilization of mine geothermal energy. *Chinese Journal of Engineering*, 44(10):1632–1651, 2022.

[12] Zhaoxiang Chu, Kaijun Dong, Penghui Gao, Yijiang Wang, and Qin Sun. Mine-oriented low-enthalpy geothermal exploitation: A review from spatio-temporal perspective. *Energy Conversion and Management*, 237:114123, 2021.

[13] Kathrin Kranz and Julia Dillenardt. Mine water utilization for geothermal purposes in freiberg, germany: determination of hydrogeological and thermophysical rock parameters. *Mine Water and the Environment*, 29:68–76, 2010.

[14] Ralph Matthes and Jochen Schreyer. Remediation of the old wismut-shaft 302 in marienberg and installation of a technical plant for geothermic mine water use (ore mountains, germany). pages 227–231, 2007.

[15] Julien Mouli-Castillo, Jeroen van Hunen, Michael MacKenzie, Thomas Sear, and Charlotte Adams. Gemstoolbox: A novel modelling tool for rapid screening of mines for geothermal heat extraction. *Applied Energy*, 360:122786, 2024.

[16] Man-chao He. Application of hems cooling technology in deep mine heat hazard control. *Mining Science and Technology (China)*, 19(3):269–275, 2009.

[17] Pingye Guo, Guolong Zhu, and Manchao He. Hems technique for heat-harm control and geothermal utilization in deep mines. *International Journal of Coal Science & Technology*, 1(3):289–296, 2014.

[18] Yu Xu, Zijun Li, Yin Chen, Mintao Jia, Mengsheng Zhang, and Rongrong Li. Synergetic mining of geothermal energy in deep mines: An innovative method for heat hazard control. *Applied Thermal Engineering*, 210:118398, 2022.

[19] Yu Xu, Zijun Li, Ming Tao, Saeid Jalilinasrabady, Junjian Wang, Gang Li, and Kaiqi Zhong. An investigation into the effect of water injection parameters on synergetic mining of geothermal energy in mines. *Journal of Cleaner Production*, 382:135256, 2023.

[20] Wenzhuo Cao, Ji-Quan Shi, Sevket Durucan, and Anna Korre. Evaluation of shear slip stress transfer mechanism for induced microseismicity at in salah co2 storage site. *International Journal of Greenhouse Gas Control*, 107:103302, 2021.

[21] Luming Zhou, Zhende Zhu, Xinghua Xie, and Yunjin Hu. Coupled thermal–hydraulic–mechanical model for an enhanced geothermal system and numerical analysis of its heat mining performance. *Renewable Energy*, 181:1440–1458, 2022.

[22] Xiao-Ping Zhou, Er-Bao Du, and Yun-Teng Wang. Thermo-hydro-chemo-mechanical coupling peridynamic model of fractured rock mass and its application in geothermal extraction. *Computers and Geotechnics*, 148:104837, 2022.

[23] Yuliang Zhang and Gao-Feng Zhao. A global review of deep geothermal energy exploration: from a view of rock mechanics and engineering. *Geomechanics and Geophysics for Geo-Energy and Geo-Resources*, 6(1):4, 2020.

[24] SN Pandey, Vikram Vishal, and A Chaudhuri. Geothermal reservoir modeling in a coupled thermo-hydro-mechanical-chemical approach: A review. *Earth-Science Reviews*, 185:1157–1169, 2018.

[25] A Ghassemi. A review of some rock mechanics issues in geothermal reservoir development. *Geotechnical and Geological Engineering*, 30:647–664, 2012.

[26] Jonny Rutqvist and Ove Stephansson. The role of hydromechanical coupling in fractured rock engineering. *Hydrogeology Journal*, 11:7–40, 2003.

[27] Olaf Kolditz, Keita Yoshioka, Tuanny Cajuhi, Ralf-Michael Günther, Holger Steeb, Frank Wuttke, and Thomas Nagel. *GeomInt—Discontinuities in Geosystems From Lab to Field Scale*. Springer Nature, 2023.

[28] Y Huang, Z Lei, K Lipnikov, JD Moulton, MR Sweeney, JD Hyman, E Knight, and PH Stauffer. Modeling coupled thermo-hydro-mechanical-chemical processes in subsurface geological media. In *ARMA US Rock Mechanics/Geomechanics Symposium*, pages ARMA–2023. ARMA, 2023.

[29] Norihiro Watanabe, Wenqing Wang, Christopher I McDermott, Takeo Taniguchi, and Olaf Kolditz. Uncertainty analysis of thermo-hydro-mechanical coupled processes in heterogeneous porous media. *Computational Mechanics*, 45:263–280, 2010.

[30] Xiaomeng Song, Jianyun Zhang, Chesheng Zhan, Yunqing Xuan, Ming Ye, and Chonggang Xu. Global sensitivity analysis in hydrological modeling: Review of concepts, methods, theoretical framework, and applications. *Journal of hydrology*, 523:739–757, 2015.

[31] Alexandros Daniilidis, Sanaz Saeid, and Nima Gholizadeh Doonechaly. The fault plane as the main fluid pathway: Geothermal field development options under subsurface and operational uncertainty. *Renewable Energy*, 171:927–946, 2021.

[32] Yang Wang, Denis Voskov, Alexandros Daniilidis, Mark Khait, Sanaz Saeid, and David Bruhn. Uncertainty quantification in a heterogeneous fluvial sandstone reservoir using gpu-based monte carlo simulation. *Geothermics*, 114:102773, 2023.

[33] Alexandros Daniilidis, Hamidreza M Nick, and David F Bruhn. Interdependencies between physical, design and operational parameters for direct use geothermal heat in faulted hydrothermal reservoirs. *Geothermics*, 86:101806, 2020.

[34] Thomas Hermans, Pascal Goderniaux, Damien Jougnot, Jan Fleckenstein, Philip Brunner, Frédéric Nguyen, Niklas Linde, Johan Alexander Huisman, Olivier Bour, Jorge Lopez Alvis, et al. Advancing measurements and representations of subsurface heterogeneity and dynamic processes: towards 4d hydrogeology. *Hydrology and Earth System Sciences Discussions*, 2022:1–55, 2022.

[35] Pingye Guo, Liange Zheng, Xiaoming Sun, Manchao He, Yanwei Wang, and Jingshi Shang. Sustainability evaluation model of geothermal resources in abandoned coal mine. *Applied Thermal Engineering*, 144:804–811, 2018.

[36] Musa D Aliyu and Hua-Peng Chen. Sensitivity analysis of deep geothermal reservoir: Effect of reservoir parameters on production temperature. *Energy*, 129:101–113, 2017.

[37] Zhi-xue Sun, Xu Zhang, Yi Xu, Jun Yao, Hao-xuan Wang, Shuhuan Lv, Zhi-lei Sun, Yong Huang, Ming-yu Cai, and Xiaoxue Huang. Numerical simulation of the heat extraction in egs with thermal-hydraulic-mechanical coupling method based on discrete fractures model. *Energy*, 120:20–33, 2017.

[38] Jun Yao, Xu Zhang, Zhixue Sun, Zhaoqin Huang, Junrong Liu, Yang Li, Ying Xin, Xia Yan, and Wenzheng Liu. Numerical simulation of the heat extraction in 3d-egs with thermal-hydraulic-mechanical coupling method based on discrete fractures model. *Geothermics*, 74:19–34, 2018.

[39] Jihoon Park, Guang Yang, Addy Satija, Céline Scheidt, and Jef Caers. Dgsa: A matlab toolbox for distance-based generalized sensitivity analysis of geoscientific computer experiments. *Computers & geosciences*, 97:15–29, 2016.

[40] Darryl Fenwick, Céline Scheidt, and Jef Caers. Quantifying asymmetric parameter interactions in sensitivity analysis: application to reservoir modeling. *Mathematical Geosciences*, 46:493–511, 2014.

[41] Noah D Athens and Jef K Caers. A monte carlo-based framework for assessing the value of information and development risk in geothermal exploration. *Applied Energy*, 256:113932, 2019.

[42] Ahinoam Pollack and Tapan Mukerji. What earth properties and engineering decisions most influence the productivity of an enhanced geothermal system? *Energy Procedia*, 158:6024–6029, 2019.

[43] Thomas Hermans, Frédéric Nguyen, Maria Klepikova, Alain Dassargues, and Jef Caers. Uncertainty quantification of medium-term heat storage from short-term geophysical experiments using bayesian evidential learning. *Water Resources Research*, 54(4):2931–2948, 2018.

[44] Yao Tong and Tapan Mukerji. Generalized sensitivity analysis study in basin and petroleum system modeling, case study on piceance basin, colorado. *Journal of Petroleum Science and Engineering*, 149:772–781, 2017.

[45] Aqeel Afzal Chaudhry, Jörg Buchwald, and Thomas Nagel. Local and global spatio-temporal sensitivity analysis of thermal consolidation around a point heat source. *International Journal of Rock Mechanics and Mining Sciences*, 139:104662, 2021.

[46] Xinxin Li, Chengyu Li, Wenping Gong, Yanjie Zhang, and Junchao Wang. Probabilistic analysis of heat extraction performance in enhanced geothermal system based on a dfn-based modeling scheme. *Energy*, 263:125674, 2023.

[47] Richard Hoffmann, Alain Dassargues, Pascal Goderniaux, and Thomas Hermans. Heterogeneity and prior uncertainty investigation using a joint heat and solute tracer experiment in alluvial sediments. *Frontiers in Earth Science*, 7:108, 2019.

[48] Tiankui Guo, Songjun Tang, Jiang Sun, Facheng Gong, Xiaoqiang Liu, Zhanqing Qu, and Wei Zhang. A coupled thermal-hydraulic-mechanical modeling and evaluation of geothermal extraction in the enhanced geothermal system based on analytic hierarchy process and fuzzy comprehensive evaluation. *Applied Energy*, 258:113981, 2020.

[49] Mohammadreza Mir Tamizdoust and Omid Ghasemi-Fare. A fully coupled thermo-poro-mechanical finite element analysis to predict the thermal pressurization and thermally induced pore fluid flow in soil media. *Computers and Geotechnics*, 117:103250, 2020.

[50] Víctor Vilarrasa, Sebastià Olivella, Jesús Carrera, and Jonny Rutqvist. Long term impacts of cold co2 injection on the caprock integrity. *International Journal of Greenhouse Gas Control*, 24:1–13, 2014.

[51] Seunghee Kim and Seyyed A Hosseini. Hydro-thermo-mechanical analysis during injection of cold fluid into a geologic formation. *International Journal of Rock Mechanics and Mining Sciences*, 77:220–236, 2015.

[52] Robin Thibaut, Eric Laloy, and Thomas Hermans. A new framework for experimental design using bayesian evidential learning: The case of wellhead protection area. *Journal of Hydrology*, 603:126903, 2021.

[53] Yi Xue, Shuai Liu, Junrui Chai, Jia Liu, PG Ranjith, Chengzheng Cai, Feng Gao, and Xue Bai. Effect of water-cooling shock on fracture initiation and morphology of high-temperature granite: Application of hydraulic fracturing to enhanced geothermal systems. *Applied Energy*, 337:120858, 2023.

[54] Guihong Liu, Hai Pu, Zhihong Zhao, and Yanguang Liu. Coupled thermo-hydro-mechanical modeling on well pairs in heterogeneous porous geothermal reservoirs. *Energy*, 171:631–653, 2019.

[55] Silvia De Simone, Victor Vilarrasa, Jesús Carrera, Andrés Alcolea, and Peter Meier. Thermal coupling may control mechanical stability of geothermal reservoirs during cold water injection. *Physics and Chemistry of the Earth, Parts A/B/C*, 64:117–126, 2013.

[56] Mingjie Chen, Andrew FB Tompson, Robert J Mellors, and Osman Abdalla. An efficient optimization of well placement and control for a geothermal prospect under geological uncertainty. *Applied energy*, 137:352–363, 2015.

[57] Z Perzan, T Babey, J Caers, JR Bargar, and K Maher. Local and global sensitivity analysis of a reactive transport model simulating floodplain redox cycling. *Water resources research*, 57(12):e2021WR029723, 2021.

[58] Céline Scheidt, Lewis Li, and Jef Caers. *Quantifying uncertainty in subsurface systems*, volume 236. John Wiley & Sons, 2018.

[59] Paul Segall and Shaun D Fitzgerald. A note on induced stress changes in hydrocarbon and geothermal reservoirs. *Tectonophysics*, 289(1-3):117–128, 1998.

[60] A Sackfield, DA Hills, and D Nowell. *Mechanics of elastic contacts*. Elsevier, 2013.

[61] Márton Major, Alexandros Daniilidis, Thomas Mejer Hansen, Mark Khait, and Denis Voskov. Influence of process-based, stochastic and deterministic methods for representing heterogeneity in fluvial geothermal systems. *Geothermics*, 109:102651, 2023.

[62] Xu Zhang, Cunqi Jia, Jun Yao, Zhaoqin Huang, Liang Gong, Wendong Yang, Xia Yan, and Yang Li. An evaluation framework for production performance of high-temperature fractured and karstified geothermal reservoirs: Production mechanism, sensitivity study, and key parameters ranking. *Gondwana Research*, 122:279–305, 2023.

[63] Zhiwei Ye and JG Wang. Uncertainty analysis for heat extraction performance from a stimulated geothermal reservoir with the diminishing feature of permeability enhancement. *Geothermics*, 100:102339, 2022.

[64] Yinlin Ji, Yuedu Chen, Hannes Hofmann, Yuan Zhang, Arno Zang, and Günter Zimmermann. The role of temperature-enhanced fault closure in promoting postinjection pressure diffusion and seismicity in enhanced geothermal systems. *Deep Underground Science and Engineering*, 2(4):394–405, 2023.

[65] Francesco Parisio, Victor Vilarrasa, Wenqing Wang, Olaf Kolditz, and Thomas Nagel. The risks of long-term re-injection in supercritical geothermal systems. *Nature communications*, 10(1):4391, 2019.

[66] William L Ellsworth. Injection-induced earthquakes. *science*, 341(6142):1225942, 2013.

[67] Thomas Hermans, Nolwenn Lesparre, Guillaume De Schepper, and Tanguy Robert. Bayesian evidential learning: a field validation using push-pull tests. *Hydrogeology Journal*, 27(5):1661–1672, 2019.

[68] Robin Thibaut, Nicolas Compaire, Nolwenn Lesparre, Maximilian Ramgraber, Eric Laloy, and Thomas Hermans. Comparing well and geophysical data for temperature monitoring within a bayesian experimental design framework. *Water Resources Research*, 58(11):e2022WR033045, 2022.

[69] Thomas Hermans, Erasmus Oware, and Jef Caers. Direct prediction of spatially and temporally varying physical properties from time-lapse electrical resistance data. *Water Resources Research*, 52(9):7262–7283, 2016.

[70] Hadrien Michel, Frédéric Nguyen, Thomas Kremer, Ann Elen, and Thomas Hermans. 1d geological imaging of the subsurface from geophysical data with bayesian evidential learning. *Computers & geosciences*, 138:104456, 2020.